LOCAL BUCKLING OF FRP STRUCTURAL SHAPES - EXPLICIT ANALYSES

Pizhong Qiao and Guiping Zou, The University of Akron, Akron, OH

Abstract

Pultruded Fiber-reinforced plastic (FRP) structural shapes (beams and columns) are thin-walled open or closed sections consisting of assemblies of flat panels and commonly made of E-glass fibers and polyester or vinylester resin. Due to the high strength-to-stiffness ratio of composites and thin-walled sectional geometry of FRP shapes, buckling is the most likely mode of failure before material failure. In this paper, explicit analyses of local buckling of rectangular composite plates with various unloaded edge boundary conditions (i.e., (1) rotationally restrained elastically along both unloaded edges and (2) one rotationally restrained and other free along the unloaded edges) and subjected to uniform in-plane axial action at simply supported loaded edges are presented. A variational formulation of the Ritz method is used to establish an eigenvalue problem, and by using combined harmonic and polynomial buckling deformation functions for box section and linearly combining the displacement fields of two extreme cases of simply-free and clamped-free boundary conditions for I-section, explicit solutions of plate local buckling coefficients are obtained. The two cases of elastically rotationally restrained plates are further treated as discrete plates or panels of fiber-reinforced plastic (FRP) closed and open sections, and by considering the effect of elastic restraints at the joint connections of flanges and webs, the local buckling strength of FRP shapes is predicted. The theoretical predictions are in good agreements with transcendental solutions and finite element eigenvalue analyses for local buckling of FRP columns. The present explicit formulation can be applied to determine local buckling capacities of composite plates with elastic restraints along the unloaded edges and can be further used to predict the local buckling strength of FRP shapes.

***Keywords*:** Local buckling, FRP Shapes, Explicit Design.

Introduction

Fiber-reinforced plastic (FRP) structural shapes (beams and columns) are increasingly used in civil infrastructure applications [1]. The common FRP shapes are thin-walled sections consisting of assemblies of flat panels and made of E-glass fibers and polyester or vinylester resin using pultrusion process. Due to the thin-walled sectional geometry and relatively low stiffness of FRP shapes, problems associated with local buckling are common in current design of FRP shapes [2].

In general, the local buckling analyses of FRP shapes are accomplished by modeling the flanges and webs individually and considering the flexibility of the flange-web connections. In this type of simulation, each part of FRP shapes is modeled as a plate subjected to elastic restraints along the unloaded edges (i.e., the flange-web connections) [2]. An extensive review of research on composite plate buckling behavior has been presented by Turvey and Marshall [3], and applications of discrete plate analyses for local buckling of FRP shapes have been reviewed and studied by Qiao et al. [2]. Even though significant research on local buckling of composite plates is presented in the literature, there are no simple and explicit formulations available for local buckling of elastically restrained plates, which can be further applied to predict the local buckling strength of FRP shapes.

In this paper, the explicit solutions for local buckling of FRP plates elastically restrained along the unloaded edges are considered, and two types of commonly used pultruded FRP shapes, an I-section and a box-section, are analyzed. For a box-section (Figure 1), the flange can be modeled as an anisotropic plate connected to the webs and under uniformly distributed compression loading on two opposite edges. Similarly, the flange of an FRP I-beam is simulated as a plate element with appropriate conditions as illustrated in Figure 2. By using combined harmonic and polynomial buckling deformation functions for box section and linearly combining the displacement fields of two extreme cases of simply-free and clamped-free boundary conditions for I-section, a variational approach of the Ritz method is used to establish an eigenvalue problem, and explicit solutions for local buckling of two types of elastic restrained plates (see Figures 1 and 2) are obtained. By considering the effect of elastic restraints at the flange-web joint connections of thin-walled sections, the explicit formulas of local buckling of elastically restrained plates are applied for prediction of local buckling strength of FRP shapes. The explicit predictions are compared with the exact transcendental solutions and finite element analyses of FRP sections.

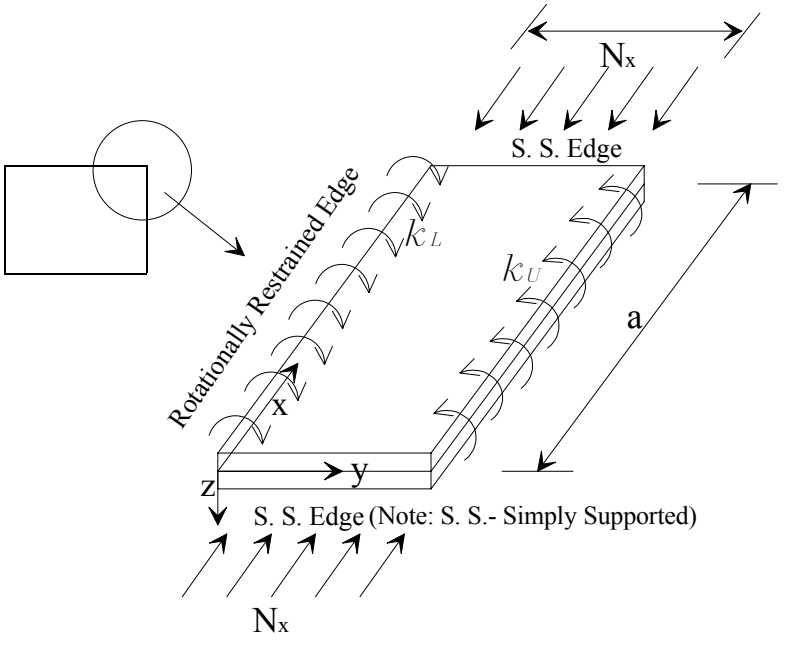

Figure 1. Geometry of idealized panel of box-section

Variational Formulation for Local Buckling of Elastically Restrained Orthotropic Plates

The local buckling of an orthotropic plate subjected to uniform in-plane axial load along the simply supported edges and rotationally restrained at two unloaded edges is briefly presented in this section. A variational formulation of the Ritz method is used herein to analyze the elastic buckling of an orthotropic plate with the boundary conditions shown in Figures 1 and 2. In the variational form of the Ritz method used in this study, the first variations of the elastic strain energy stored in the plate (δU_e), the strain energy stored in the elastic restraints along the rotationally restrained boundaries of the plate (δU_Γ), and the work done by the axial in-plane force (δV) are computed by properly chosen out-of-plane buckling displacement function (w). The elastic strain energy in an orthotropic plate (U_e) is given as

$$U_e = \frac{1}{2}\iint_{\Omega} \left\{D_{11}w_{,xx}^2 + D_{22}w_{,yy}^2 + 2D_{12}w_{,xx}w_{,yy} + 4D_{66}w_{,xy}^2\right\}dxdy \tag{1}$$

where D_{ij} (i, j = 1, 2, 6) are the plate bending stiffness coefficients [4] and Ω is the area of the plate.

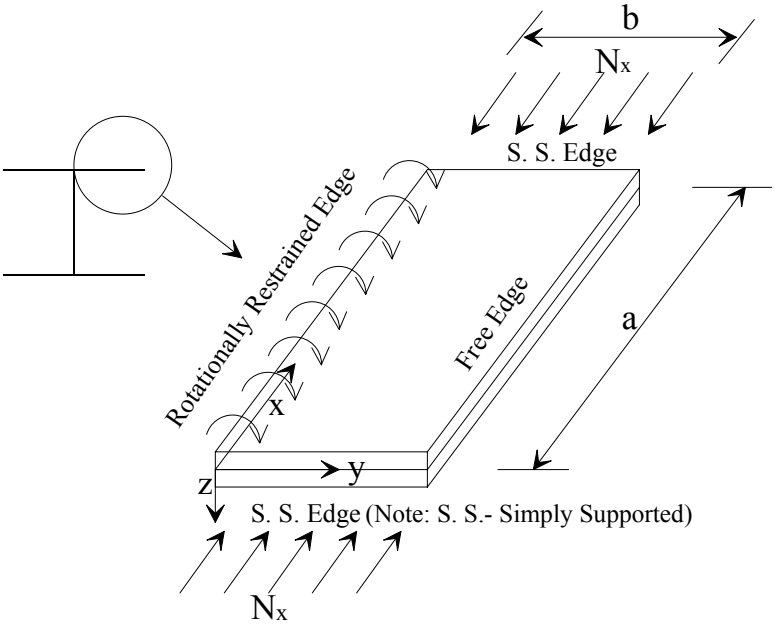

Figure 2. Geometry of idealized flange panel of wide-flange I-section

For the plate with rotational restraints distributed along the unloaded boundary edges, the strain energy (U_Γ) stored in equivalent elastic springs at the flange-web connections is given as

$$U_\Gamma = \frac{1}{2}\int_\Gamma k_L\left(\frac{\partial w}{\partial y}|_{y=0}\right)^2 d\Gamma + \frac{1}{2}\int_\Gamma k_U\left(\frac{\partial w}{\partial y}|_{y=b}\right)^2 d\Gamma \quad \text{for the plate shown in Figure 1} \tag{2}$$

$$U_\Gamma = \frac{1}{2}\int_\Gamma k\left(\frac{\partial w}{\partial y}|_{y=0}\right)^2 d\Gamma \quad \text{for the plate shown in Figure 2} \tag{3}$$

where k_L and k_U in Eq. (2) are the rotational stiffness at the edges of y = 0 and b (Figure 1), and k in Eq. (3) is the rotational stiffness of the web and the flange-web connection combined (Figure 2). Then, the corresponding first variations of strain energy stored in the elastic restraints along the rotationally restrained boundary of the plate (δU_Γ) are

$$\begin{aligned}\delta U_\Gamma = {} & k_L\int_\Gamma \left(\frac{\partial w}{\partial y}|_{y=0}\right)\delta\left(\frac{\partial w}{\partial y}|_{y=0}\right)d\Gamma \\ & + k_U\int_\Gamma \left(\frac{\partial w}{\partial y}|_{y=b}\right)\delta\left(\frac{\partial w}{\partial y}|_{y=b}\right)d\Gamma\end{aligned} \quad \text{for the plate shown in Figure 1} \tag{4}$$

$$\delta U_\Gamma = k\int_\Gamma \left(\frac{\partial w}{\partial y}|_{y=0}\right)\delta\left(\frac{\partial w}{\partial y}|_{y=0}\right)d\Gamma \quad \text{for the plate shown in Figure 2} \tag{5}$$

The work done (V) by in-plane uniformly distributed compressive force (N_x) can be written as

$$V = \frac{1}{2}N_x\iint_\Omega w_{,x}^2 dxdy \tag{6}$$

where N_x is defined as the compressive force per unit length at the simply supported boundary of $x = 0$ and a.

Explicit Solutions for Local Buckling

To solve the eigenvalue problem, it is very important to choose proper out-of-plane buckling displacement function (w). In this paper, to explicitly obtain the analytical solutions for local buckling of two types of representative plates corresponding to the box and I sections, respectively, (see Figures 1 and 2), the unique buckling displacement fields are proposed.

As shown in Figure 1, the boundary conditions along rotationally restrained unloaded edge are written as

$$w(x,0) = 0 \tag{7a}$$

$$w(x,b) = 0 \tag{7b}$$

$$M_y(x,0) = -D_{22}\left(\frac{\partial^2 w}{\partial y^2}\right)_{y=0} = -k_L\left(\frac{\partial w}{\partial y}\right)_{y=0} \tag{7c}$$

$$M_y(x,b) = -D_{22}\left(\frac{\partial^2 w}{\partial y^2}\right)_{y=b} = -k_U\left(\frac{\partial w}{\partial y}\right)_{y=b} \tag{7b}$$

While as shown in Figure 2, the boundary conditions along the flange-web connection or rotationally restrained unloaded edge are written as

$$w(x,0) = 0 \tag{8a}$$

$$\theta(x,0) = \left(\frac{\partial w}{\partial y}\right)_{y=0} = \bar{\theta} \tag{8b}$$

$$M_y(x,0) = -D_{22}\left(\frac{\partial^2 w}{\partial y^2}\right)_{y=0} = -k\left(\frac{\partial w}{\partial y}\right)_{y=0} \tag{8c}$$

The assumed plate displacement function which satisfy all the restrained boundary conditions shown in Figure 1 is stated as

$$\begin{aligned} w(x,y) = \{&\frac{y}{b} + \frac{\chi_L y^2}{2b} - \frac{(12+5\chi_L+3\chi_U+\chi_L\chi_U)y^3}{(6+\chi_U)b^3} \\ &+ \frac{(12+4\chi_L+4\chi_U+\chi_L\chi_U)y^4}{2(6+\chi_U)b^4}\} \cdot \sum_{m=1}^{\infty} \alpha_m \sin\frac{m\pi x}{a} \end{aligned} \tag{9}$$

where, χ_L and χ_U are the coefficients of elastic restraint at the unloaded edges ($y = 0$ and b, respectively) and expressed as:

$$\chi_L = k_L b / D_{22},\ \chi_U = k_U b / D_{22} \tag{10}$$

and noting that k_L and k_U are all positive values, as given in Eq. (9); χ_L or $\chi_U = 0$ (k_L or $k_U = 0$) corresponds to the simply-supported boundary at rotationally restrained edges of $y = 0$ or $y = b$; whereas, χ_L or $\chi_U = \infty$ (k_L or $k_U = \infty$) correspond to the clamped boundary at rotationally restrained edges.

As shown in Figure 2 for the discrete plate (flange) of I-sections, a new buckling displacement w which linearly combines the simply-free (SF) and clamped-free (CF) boundary buckling displacements and satisfies all the restrained boundary conditions is proposed as

$$w(x,y)=\left\{(1-\frac{bk}{2D_{22}+bk})\frac{y}{b}+\frac{bk}{2D_{22}+bk}\left(\frac{y}{b}\right)^2\right\}\cdot\sum_{m=1}^{\infty}\alpha_m\sin\frac{m\pi x}{a} \tag{11}$$

As given in Eq. (11), $k = 0$ (simply-supported at rotationally restrained edge) corresponds to the plate with the SF boundary condition along the unloaded edges; whereas, $k = \infty$ (clamped at rotationally restrained edge) refers to the one with the CF boundary condition. For $0 < k < \infty$, the restrained-free (RF) condition at unloaded edges is taken into account in the formulation.

By substituting Eq. (9) into Eqs. (1), (2) and (6), the elastic strain energy in the plate (U_e), strain energy in the elastic restraints along the rotationally restrained boundary of the plate (U_Γ), and work done by the axial in-plane compressive force (V) are derived, respectively. By differentiating the total energy which is the sum of strain energy, restrained energy and work done under in-plane compressive loads leads to the solution of an eigenvalue problem of which order is simply a unity. Hence after some numerical symbolic computation, the local buckling coefficient (see Figure 1) can be explicitly expressed as

$$\begin{aligned}\beta=&\frac{10080(6+\chi_U)^2}{(\eta_{10}\chi_L^2+2\eta_{11}\chi_L+2\eta_{12})}\{\frac{\gamma^2\chi_L}{2m^2\pi^4}+\frac{\gamma^2(6+\chi_L)^2\chi_U}{2m^2\pi^4(6+\chi_U)^2}\\&+\frac{\gamma^2(\eta_4\chi_L^2+4\eta_5\chi_L+36\eta_6)}{2m^2\pi^4(6+\chi_U)^2}+\frac{(D_{12}+2D_{66})(\eta_8\chi_L^2+3\eta_8\chi_L+72\eta_9)}{210\pi^2(6+\chi_U)^2D_{22}}\\&+\frac{m^2D_{11}(\eta_1\chi_L^2+\eta_2\chi_L+4\eta_3)}{5040\gamma^2(6+\chi_U)^2D_{22}}\}\end{aligned} \tag{12}$$

where $\gamma = a/b$ is the aspect ratio of the plate. The plate compressive local buckling load (Nx, see Figure 1) (force per unit length) can be written in term of the local buckling coefficient as

$$N_x=\frac{\beta\pi^2D_{22}}{b^2} \tag{13}$$

By minimizing Eq. (12) with respect to the aspect ratio ($\gamma = a/b$) (i.e., $d\beta/d\gamma = 0$), the respective critical aspect ratio and critical local buckling coefficient can be established as

$$\gamma_{cr}=0.663\left\{\frac{m^4(\eta_1\chi_L^2+\eta_2\chi_L+4\eta_3)D_{11}}{(\eta_{13}\chi_L^2+\eta_{14}\chi_L+36\eta_{15})D_{22}}\right\}^{\frac{1}{4}} \tag{14}$$

and

$$\begin{aligned}\beta_{cr}=&\frac{24}{\pi^2D_{22}(\eta_{10}\chi_L^2+2\eta_{11}\chi_L+2\eta_{12})}\{2(D_{12}+2D_{66})(\eta_7\chi_L^2+3\eta_8\chi_L+72\eta_9\\&+3.742\sqrt{D_{11}D_{22}(\eta_1\chi_L^2+\eta_2\chi_L+4\eta_3)(\eta_{13}\chi_L^2+\eta_{14}\chi_L+36\eta_{15})}\}\end{aligned} \tag{15}$$

where

$$\begin{aligned}\eta_1&=76+17\chi_U+\chi_U^2,\eta_2=1140+272\chi_U+17\chi_U^2,\eta_3=1116+285\chi_U+19\chi_U^2\\\eta_4&=36+8\chi_U+\chi_U^2,\eta_5=54+9\chi_U+2\chi_U^2,\quad\eta_6=24+6\chi_U+19\chi_U^2\\\eta_7&=72+15\chi_U+\chi_U^2,\eta_8=312+70\chi_U+5\chi_U^2,\eta_9=51+13\chi_U+\chi_U^2\\\eta_{10}&=152-86\sigma+(34-18\sigma)\chi_U+(2-\sigma)\chi_U^2,\eta_{13}=36+13\chi_U+\chi_U^2\\\eta_{11}&=12(95-51\sigma)+136(2-\sigma)\chi_U+(17-8\sigma)\chi_U^2,\eta_{14}=396+156\chi_U+13\chi_U^2\\\eta_{12}&=2232(2-\sigma)+12(95-44\sigma)\chi_U+(76-33\sigma)\chi_U^2,\eta_{15}=24+11\chi_U+\chi_U^2\end{aligned} \tag{16}$$

Noting that Eq. (16) is independent of the number of buckling half-wave length (m). Finally, the critical local buckling load or the critical local buckling stress resultant for orthortropic plates with the rotationally restrained-restrained (RR) condition (for the plate with loading and boundary conditions shown in Figure 1) can be expressed as

$$\left(N_x\right)_{cr} = \frac{\beta_{cr}\pi^2 D_{22}}{b^2} \quad \text{for the plate shown in Figure 1} \tag{17}$$

Similarly, by substituting Eq. (11) into Eqs. (1), (3) and (6) and after some numerical symbolic computation, the local buckling coefficient for the plate with the loading and boundary conditions shown in Figure 2 can be explicitly expressed as

$$\begin{aligned}\beta = {} & \frac{60\gamma^2(-1+\omega)^2}{m^2\pi^4\xi(10-5\omega+\omega^2)} + \frac{120\omega^2\gamma^2}{m^2\pi^4(10-5\omega+\omega^2)} + \frac{m^2 D_{11}}{\gamma^2 D_{22}} \\ & + \frac{20(-3+\omega)\omega D_{12}}{\pi^2(10-5\omega+\omega^2)D_{22}} + \frac{40(3+\omega^2)D_{66}}{\pi^2(10-5\omega+\omega^2)D_{22}}\end{aligned} \tag{18}$$

where

$$\gamma = \frac{a}{b};\ \ \xi = \frac{2D_{22}}{bk};\ \omega = \frac{1}{1+\xi} \tag{19}$$

and $\gamma = a/b$ is the aspect ratio of the plate, and ξ is the coefficient of elastic restraint which depend on the properties of flange-web connection [2]. Again, $\xi = \infty$ (or $\omega = 0$ and $k = 0$) is for the case of the plate simply-supported at the rotationally restrained unloaded edge; whereas, $\xi = 0$ (or $\omega = 1$ and $k = \infty$) is for the one clamped.

By minimizing Eq. (18) with respect to the aspect ratio ($\gamma = a/b$) (i.e., $d\beta / d\gamma = 0$), the respective critical aspect ratio and critical local buckling coefficient can be established as

$$\gamma_{cr} = 1.1287m\left\{\frac{\xi(10-5\omega+\omega^2)D_{11}}{[(-1+\omega)^2+2\omega^2]D_{22}}\right\}^{\frac{1}{4}} \tag{20}$$

and

$$\begin{aligned}\beta_{cr} = {} & \frac{20(-3+\omega)\omega D_{12}}{\pi^2(10-5\omega+\omega^2)D_{22}} + \frac{2\sqrt{15}(-1+\omega)^2\sqrt{\xi(10-5\omega+\omega^2)D_{11}}}{\pi^2\xi(10-5\omega+\omega^2)\sqrt{[(-1+\omega)^2+2\omega^2]D_{22}}} + \frac{40(3+\omega^2)D_{66}}{\pi^2(10-5\omega+\omega^2)D_{22}} \\ & + \frac{2\sqrt{15}D_{11}\sqrt{[(-1+\omega)^2+2\omega^2]D_{22}}}{\pi^2 D_{22}\sqrt{\xi(10-5\omega+\omega^2)D_{11}}} + \frac{4\sqrt{15}\omega^2\sqrt{\xi(10-5\omega+\omega^2)D_{11}}}{\pi^2(10-5\omega+\omega^2)\sqrt{[(-1+\omega)^2+2\omega^2]D_{22}}}\end{aligned} \tag{21}$$

Noting that Eq. (21) is independent of the number of buckling half-wavelength (m). Finally, the critical local buckling load or the critical stress resultant for orthotropic plates with the RF condition (for the plate condition shown in Figure 1) can be expressed as

$$\left(N_x\right)_{cr} = \frac{\beta_{cr}\pi^2 D_{22}}{b^2} \quad \text{for the plate shown in Figure 2} \tag{22}$$

or explicitly in term of the coefficient of elastic restraint (ξ),

$$\begin{aligned}\left(N_x\right)_{cr} = {} & \frac{1}{b^2(6+15\xi+10\xi^2)}\left[-20(2+3\xi)D_{12} + 15.49\sqrt{(2+\xi)}\sqrt{(6+15\xi+10\xi^2)}\sqrt{D_{11}D_{22}}\right. \\ & \left. + 40(4+6\xi+3\xi^2)D_{66}\right]\end{aligned} \tag{23}$$

Based on the explicit formulas in Eqs. (17) and (22), design formulas of critical local buckling load for several common cases of applications are summarized as follows:

Case 1: Plates with two simply-supported unloaded edges (SS)

For the case of $\chi_L = \chi_U = 0$ ($k_L = k_U = 0$) and $\sigma = 0$ (i.e., the four edges are simply-supported and the plate is subjected to an uniformly distributed compression load in *x*-direction) (Figure 1), the explicit critical local buckling load can be simplified as

$$N_{cr} = \frac{19.742}{b^2}\{\sqrt{D_{11}D_{22}} + (D_{12} + 2D_{66})\} \tag{24}$$

Eq. (24) is identical to the one reported by Qiao et al. [2].

Case 2: Plates with two clamped unloaded edges (CC)

For the case of $\chi_L = \chi_U = \infty$ (or $k_L = k_U = \infty$) and $\sigma = 0$ (i.e., the two unloaded edges at $y = 0$ and b are clamped and the plate is subjected to uniformly distributed compressive load at simply supported edges of $x = 0$ and a) (Figure 1), the explicit critical buckling load can be simplified as

$$N_{cr} = \frac{24}{b^2}\{1.871\sqrt{D_{11}D_{22}} + (D_{12} + 2D_{66})\} \tag{25}$$

Case 3: Plates with two equal rotational restraints along unloaded edges (RR)

For the case of $\chi_L = \chi_U = \chi$ ($k_L = k_U = k$) and $\sigma = 0$ (i.e., the two unloaded edges at $y = 0$ and y = b are subjected to the same rotational restraints, and the plate is simply-supported and subjected to the uniformly distributed compression load at the edges of $x = 0$ and $x = a$) (Figure 1), the explicit critical local buckling load is given as

$$N_{cr} = \frac{24}{b^2}\{1.871\sqrt{\frac{\tau_2}{\tau_1}}\sqrt{D_{11}D_{22}} + \frac{\tau_3}{\tau_1}(D_{12} + 2D_{66})\} \tag{26}$$

where, the coefficients of τ_1, τ_2, and τ_3 are functions of elastic restraint coefficient χ, and defined as

$$\tau_1 = 124 + 22\chi + \chi^2, \tau_2 = 24 + 14\chi + \chi^2, \tau_3 = 102 + 18\chi + \chi^2 \tag{27}$$

Case 4: Plates with simply-supported and free unloaded edges (SF)

For the case of $\xi = \infty$, the simply-supported boundary at one unloaded edge is achieved. The problem is corresponding to the plate under the uniformly distributed compression load at simply-supported loaded edges and subjected to the SF boundary conditions (Figure 2), and the local buckling [$(N_x)_{cr}^{\infty}$] can be obtained as

$$(N_x)_{cr}^{\infty} = \frac{12D_{66}^f}{(b^f)^2} \tag{28}$$

Case 5: Plates with clamped-supported and free unloaded edges (CF)

For the case of $\xi = 0$, the boundary is related to clamped-supported at one unloaded edge and free at another unloaded edge (CF condition) (Figure 2), and the local buckling load can be obtained as

$$(N_x)_{cr}^{0} = \frac{4(-5D_{12} + 3\sqrt{5D_{11}D_{22}} + 20D_{66})}{3(b^f)^2} \tag{29}$$

Case 6: Plates with elastically retrained and free unloaded edges (RF)

The formula for the local buckling load of the general case of elastically restrained at one unloaded edge and free at the other (RF) (Figure 2) is given in Eq. (23).

Determination of Restraint Coefficient

The non-dimensional coefficient of elastic restraint χ in Case 3 need to be determined so that the critical buckling stress resultants N_{cr} can be predicted. As shown in Figure 1 for the box-sections, the webs are assumed to elastically restrain the flanges, and based on the derivations for the isotropic case [5] and orthotropic case [2], the rotational restraint coefficient for the box-sections is modified as

$$\chi = \frac{D_{22}^{w}}{D_{22}^{f}} \cdot \frac{r}{\rho(b^{w}/b^{f})} \tag{30}$$

where

$$r = 1 - \frac{(b^{w})^{2}}{(b^{f})^{2}} \cdot \frac{(\sqrt{D_{11}^{f} D_{22}^{f}} + D_{12}^{f} + 2D_{66}^{f})}{(\sqrt{D_{11}^{w} D_{22}^{w}} + D_{12}^{w} + 2D_{66}^{w})}, \quad \rho(b^{w}/b^{f}) = \frac{1}{\pi}\tanh(\frac{\pi b^{w}}{2b^{f}})[1 + \frac{2b^{w}/b^{f}}{\sinh(\pi b^{w}/b^{f})}] \tag{31}$$

and the superscripts *f* and *w* refer to the flange and web panels. $\chi = 0$ and $\chi = \infty$ correspond to the elastic restraints of simply supported (Case 1) and fully restrained (clamped) (Case 2) boundary conditions, respectively.

Similarly, the non-dimensional coefficient of elastic restraint (ξ) for I-sections (Figure 2), can be expressed in terms of the material and geometrical properties of the flange and web as [2, 5]:

$$\xi = \frac{\dfrac{2b^{w}}{b^{f}} \cdot \dfrac{D_{22}^{f}}{D_{22}^{w}}}{\left[1 - 0.106 \dfrac{(b^{w})^{2}}{(b^{f})^{2}} \dfrac{(\sqrt{D_{11}^{f} D_{22}^{f}} + D_{12}^{f} + 2D_{66}^{f})}{(\sqrt{D_{11}^{w} D_{22}^{w}} + D_{12}^{w} + 2D_{66}^{w})}\right]} \tag{32}$$

Using the coefficient of elastic restrain in Eq. (32), the local buckling load for Case 6 can be determined. Again, $\xi = \infty$ and $\xi = 0$ correspond to the elastic restraints of simply supported (Case 4) and fully restrained (clamped) (Case 5) boundary conditions at the flange-web connection, respectively.

Application to Local Buckling of FRP Shapes

Box-sections

As an application, the proposed formula [Eq. (17)] is applied for the local buckling predictions of four FRP box-sections (10.2×20.3×0.64 cm, 10.2×15.2×0.64 cm, 10.2×10.2×0.64 cm, and 15.2×15.2×0.95 cm). The panel material properties and corresponding elastic restraints are given in Table 1. Due to equal lengths of flanges and webs in the box-sections of 10.2×10.2×0.64 cm and 15.2×15.2×0.95 cm, the elastic restraint coefficients $\chi = 0$, and they indicate that the panels of two sections can be simplified as simply-supported plates along the unloaded edges (Case 1) and the flange and web panel components are buckled simultaneously. The present explicit solutions are compared with the exact solutions by solving the transcendental equations [2] and the finite element eigenvalue analyses by using ANSYS four-node layered shell element (SHELL 63) (Table 2), and an excellent agreement between the propsed explicit formula [Eq. (17)] and transcendental solutions is obtained. Further, the relationship of flange critical local buckling load with respect to the coefficient of elastic restraint (χ) for box-section 10.2×20.3×0.64 cm is plotted in Figure 3; while the local buckling load versus the aspect ratio (γ) of span length to width with different coefficients of elastic restraint is shown in Figure 4. It indicates that the actual value of the critical local buckling load of panel elements with consideration of elastic restraint of the flange-web connection lies between the simply-supported and fully restraint (clamped) conditions (See Table 2 and Figure 3). Also as demonstrated in Figure 4, the

local buckling load increases as the coefficient of elastic restraint increases. For the plates with lower aspect ratios, the difference of local buckling loads between the simply-supported and clamped conditions diminishes.

Table 1. Flange Panel Bending Stiffness and Elastic Restraint Coefficients for Box-Sections

Section (cm)	D_{11} (N.cm)	D_{12} (N.cm)	D_{22} (N.cm)	D_{66} (N.cm)	χ
10.2×20.3×0.64	44,370	10,340	46,070	10,680	4.271
10.2×15.2×0.64	46,860	13,770	35,000	10,740	2.934
10.2×10.2×0.64	46,860	13,770	35,000	10,740	0
12.7×12.7×0.95	164,800	29,240	101,400	28,000	0

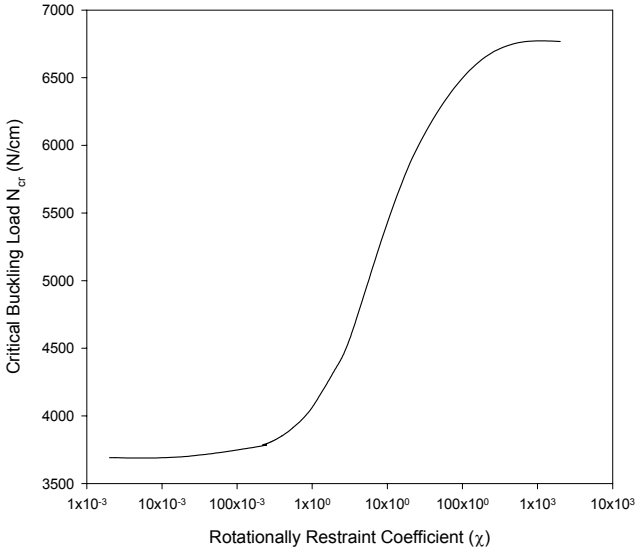

Figure 3. Effect of coefficient of elastic restraint on critical local buckling load for FRP box-section

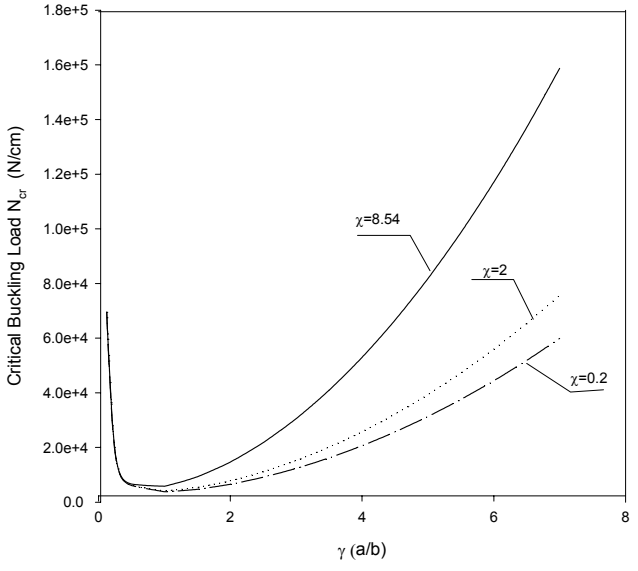

Figure 4. Effect of aspect ratio on critical local buckling load for FRP box-section

Table 2. Comparisons of Critical Local Buckling Stress Resultants for Four Box-Sections

Section (cm)	Explicit Solution (N/cm)	Transcendental Solution (TS) (N/cm)	FEM (N/cm)	Percent Difference (%) (Explicit vs TS)	Percent Difference (%) (Explicit vs EM)
10.2×20.3×0.64	4,773	4,768	4,810	0.105	-0.769
10.2×15.2×0.64	7,814	7,805	7,740	0.115	0.956
10.2×10.2×0.64	14,450	14,449	14,030	0.007	3.000
12.7×12.7×0.95	26,860	26,748	26,090	0.419	3.000

I-sections

As an application, the formulated explicit formula [Eq. (23)] is used to predict the local buckling strengths of four pultruded FRP wide-flange (WF) sections loaded axially as columns. These WF sections were experimental studied by Barbero [6]. The flange local buckling of each WF section is predicted using the present explicit formula, and the results are correlated with experimental data [6], transcendental solutions [2], and finite element eigenvalue simulations. The flange material properties [6] of the sections are listed in Table 3, and the coefficients of elastic restraint are computed using Eq. (32) (see Table 4). As indicated in Table 4, the present explicit solutions of critical stress resultants compare closely with theoretical predictions by transcendental solutions, experimentally measured values and finite element eigenvalue analytical results. Also as illustrations, the local buckling coefficient (β) versus the aspect ratio (γ) with different coefficients of elastic restraint is provided in Figure 5; while the flange local buckling pattern along with the experimental data and finite element predictions is shown in Figure 6 for WF-section 102 × 102 × 6.6 *mm* with the corresponding elastic restraints of $\xi = 6.70$. Based on Table 4, it can be concluded that the present explicit solution is highly accurate and can be used with confidence in local buckling design of FRP WF-sections.

Table 3. Flange Panel Bending Properties for Four WF-sections

Section (mm)	D_{11} $(N \cdot cm)$	D_{12} $(N \cdot cm)$	D_{22} $(N \cdot cm)$	D_{66} $(N \cdot cm)$
102×102×6.4	69,823	12,739	32,633	10,329
152×152×6.4	75,112	14,138	35,533	11,234
152×152×9.5	243,600	41,400	106,511	34,465
203×203×9.5	250,080	41,575	107,090	34,710

Table 4. Comparisons of Critical Stress Resultants for Four WF Sections

Section (mm)	Elastic restraint (ξ)	$(N_x)_{cr}^{\text{Trans.}}$ (N/cm)	$(N_x)_{cr}^{\text{FEM}}$ (N/cm)	$(N_x)_{cr}^{\text{Exp.}}$ (N/cm)	$(N_x)_{cr}^{\text{Present}}$ (N/cm)	Percent Difference (%) (Explicit vs FEM)	Percent Difference (%) (Explicit vs Exp.)
102×102×6.4	6.70	8,044	8,235	8,056	8,283	3.0	2.8
152×152×6.4	6.70	3,923	3,882	3,925	4,045	3.1	3.1
152×152×9.5	6.44	12,255	11,886	12,805	12,635	3.1	-1.3
203×203×9.5	6.44	6,959	6,568	6,668	7,167	3.0	7.0

Note: Trans – transcendental solutions; FEM – Finite element method; Exp. – Experimental results.

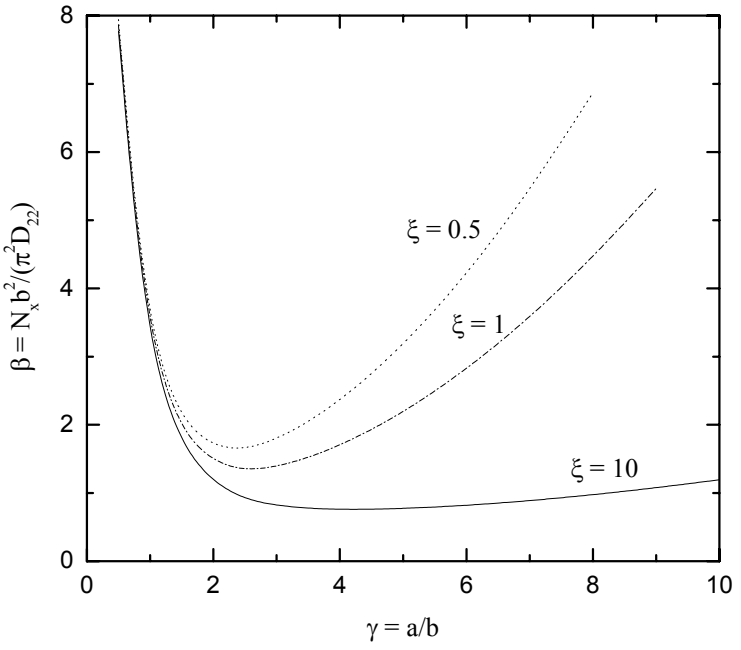

Figure 5. Local buckling coefficient vs. aspect ratio for FRP WF-section

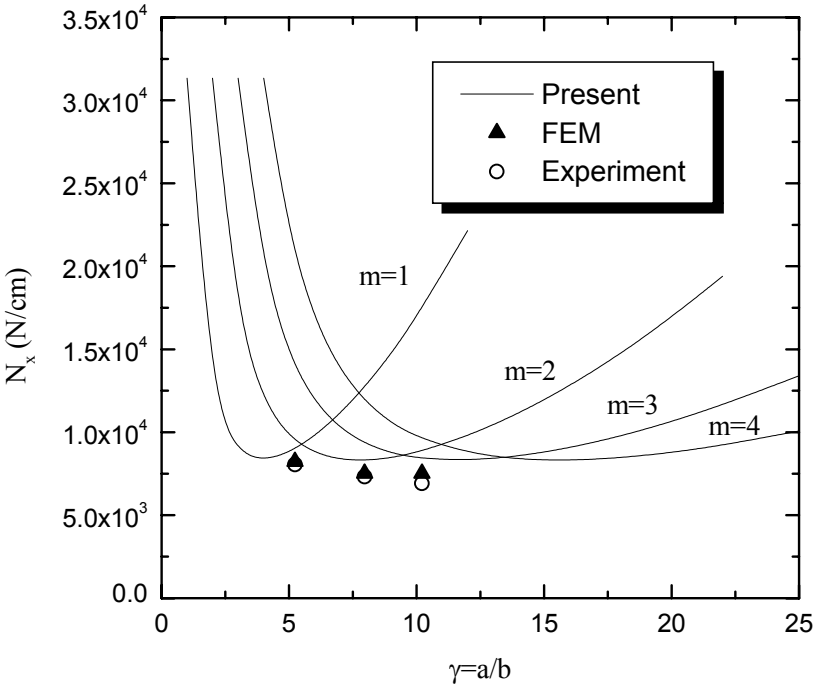

Figure 6. Flange local buckling of WF-section with $\xi = 6.70$

Conclusions

An explicit elastic stability analysis is presented for local buckling of orthotropic plates rotationally restrained elastically along unloaded edges and subjected to uniform axial loading, and the analytical solutions are extended to predict the local buckling strength of elastically restrained laminated

flange panels of FRP box-sections and wide-flange I-sections with elastic rotational restraints at the flange-web connections. By combining the harmonic and polynomial buckling deformation functions which are satisfied all the restraint boundary conditions, the effects of elastic restraints along the unloaded or at the flange-web connection are considered for the box-sections. By linearly combining the displacement fields of two extreme cases of simply-free and clamped-free boundary conditions, a new buckling displacement field for rotationally restrained-free boundary condition at the unloaded edges is developed for the wide-flange sections. A variational formulation of the Ritz method is used to establish an eigenvalue problem, and a simplified explicit flange local buckling loads for the box-sections and wide-flange sections are derived. The predictions by present explicit formulas are compared well with the transcendental solutions and finite element eigenvalue simulations for local buckling of FRP box and wide-flange sections. The explicit formulas of critical local buckling strength can be easily applied in local buckling design of FRP structural shapes.

Acknowledgements

This study was partially supported by the Ohio Board of Regents and the College of Engineering at the University of Akron. We appreciate the support and encouragement of Dr. S. Graham Kelly, Dean of the College of Engineering at the University of Akron.

References

1. Qiao, P. Z., Davalos, J. F., Barbero, E. J., and Troutman, D. L. (1999). 'Equations facility composite design." *Modern Plastics Mag.,* 76(11), 77-80.
2. Qiao, P. Z., Davalos, J. F., and Wang, J. L. (2001). "Local buckling of composite FRP shapes by discrete plate analysis." *ASCE J. Struct. Engrg.*, 127(3), 245-255.
3. Turvey, G. J., and Marshall, I. H., eds. (1995). *Buckling and postbuckling of composite plates*, Chapman & Hall, London.
4. Jones, R. M. (1975). *Mechanics of composite materials*, Hemisphere Publishing, New York.
5. Bleich, F. (1952). *Buckling strength of metal structures*, McGraw-Hill, New York.
6. Barbero, E. J. (1992). "Buckling of FRP columns." *Final Rep. Prepared for Creative Pultrusions, Inc.*, Department of Mechanical and Aerospace Engineering, West Virginia University, Morgantown. W. Va.